JOURNAL OF SPACECRAFT AND ROCKETS
Vol. 42, No. 5, September–October 2005

Using NASA Standard Breakup Model to Describe Low-Velocity Impacts on Spacecraft

Toshiya Hanada* and Tetsuo Yasaka†
Kyushu University, Fukuoka 812-8581, Japan
Hidehiro Hata‡
Kumamoto University, Kumamoto 860-8555, Japan
and
Yasuhiro Akahoshi§
Kyushu Institute of Technology, Kitakyushu 804-8550, Japan

The applicability is examined of the hypervelocity collision model included in the NASA standard breakup model 2000 revision to low-velocity collisions possible in space, especially in the geosynchronous regime. The analytic method used in the standard breakup model is applied to experimental data from low-velocity impact experiments previously performed at Kyushu University at a velocity range less than 300 m/s. The projectiles and target specimens used were stainless steel balls and aluminum honeycomb sandwich panels with face sheets of carbon fiber reinforced plastic, respectively. It is concluded that the hypervelocity collision model in the standard breakup model can be applied to low-velocity collisions with some simple modifications.

Nomenclature

A/M	=	area-to-mass ratio, m^2/kg
$D_{A/M}(\chi, \nu)$	=	area-to-mass distribution function of χ and ν
$D_{\Delta V}(\lambda_C, \chi)$	=	delta velocity distribution function of λ_C and χ
L_C	=	characteristic length, m
M	=	mass, kg
$N(L_C)$	=	size distribution function of L_C
$N(x; \mu, \sigma)$	=	Gaussian (normal) distribution in x about the mean value μ with a standard deviation of σ
S	=	dimensionless scale factor
x, y, z	=	fragment three dimensions, m
ΔV	=	delta velocity, m/s
λ_C	=	$\log(L_C)$
μ	=	mean
ν	=	$\log(\Delta V)$
ρ	=	material density, kg/m^3
σ	=	standard deviation
ϕ	=	dispersion path angle with respect to projectile in-coming velocity
χ	=	$\log(A/M)$

Introduction

SPACE structures may encounter impact phenomena in orbit. Apart from mission related collision at rendezvous or deployment, the important phenomena to be considered are collisions with exterior objects such as meteoroids and artificial debris. These objects normally collide at very high velocity, potentially causing fatal damages to space structures and the further creation of many more fragments, which then can be threats to other spacecraft in other orbits. These hypervelocity impact phenomena have been extensively studied both theoretically and experimentally, for example, by Bess,[1] Nebolsine et al.,[2] Kling,[3,4] Johnson,[5] and McKnight et al.[6,7]

The protection schemes of space structures, especially that of the International Space Station, is fairly well defined by now. The protection device is known as Whipple bumper, which is a thin wall placed in front of the main structure at a sufficient distance. At impact, much of the projectile kinetic energy is consumed during the material phase change process of both projectile and the bumper wall, and then the remaining energy is scattered into a larger area by the time the projectile remnant reaches the main structure. Because of this, the protection device is effective against a high-velocity impact. At lower velocity, the projectile just penetrates the protection wall, and then makes almost direct impact onto the main structure. The low-velocity impact phenomena are not well understood despite the mechanism of destruction being simpler.

Most collisions in low Earth orbit (LEO) are hypervelocity collisions. Impact velocity is defined by the difference of velocity vectors of two colliding objects. The scalar velocity V is expressed in terms of the magnitude of object velocities before impact, V_1 and V_2, and an angle between two velocity vectors, θ, as

$$V^2 = V_1^2 + V_2^2 - 2V_1V_2\cos\theta$$

If the two objects are flying toward the same direction ($\theta = 0$), the collision velocity becomes minimal. On the other hand, if a head-on collision occurs ($\theta = 180$), the maximum collision velocity occurs. Collision probability of an object with other objects is given by the product of collision cross-sectional area, spatial density, time, and relative velocity between the colliding objects. Therefore, if the external objects are distributed randomly, collisions at the leading edge, where the head-on collisions may occur, are most frequent, whereas those at the trailing edge are scarce.

Artificial objects in geostationary Earth orbit (GEO) are distributed differently. Most of them are originally placed on the equatorial plane, and then they change orbital plane due to the lunar and solar gravitational perturbations combined with the Earth's oblateness. The change in inclination starts at a rate of about 0.8 deg per year but shifts the direction of the change after the inclination reaches the maximum of 15 deg by 27 years (Ref. 8). If a satellite under north–south station keeping is to be hit by another artificial

Received 16 June 2004; revision received 25 October 2004; accepted for publication 3 November 2004.

*Associate Professor, Space Environment Research Center, 10-1 Hakozaki 6-chome, Higashi-ku; toshi@aero.kyushu-u.ac.jp. Senior Member AIAA.
†Professor, Department of Aeronautics and Astronautics, 10-1 Hakozaki 6-chome, Higashi-ku; yasaka@aero.kyushu-u.ac.jp. Senior Member AIAA.
‡Research Associate, Department of Mechanical Engineering, 39-1 Kurokami 2-chome; hata@mech.kumamoto-u.ac.jp.
§Associate Professor, Department of Mechanical Engineering, 1-1 Sensui-cho, Tobata-ku; akaho@mech.kyutech.ac.jp.

object, the angle of collision must be less than 15 deg. Semimajor axis and eccentricity are also subject to various perturbations, but variation of these elements is not significant. All orbits are essentially circular at nominal geostationary altitude. Objects in inclined orbits make a daily excursion in north–south direction relative to stationary satellites. Because the orbital velocity is about 3 km/s, the collision velocity is less than 800 m/s. Therefore, most collisions in GEO would be low-velocity collisions. Note that when a collision between a GEO satellite and an object in geostationary transfer orbit (GTO) is considered, the collision velocity is raised to 1.5 km/s, which corresponds with the required delta velocity to insert a satellite into GEO from GTO.

Harada[9] and Goto[10] investigated these low-velocity impact phenomena possible in GEO though laboratory experiments to establish a mathematical model to describe the fragment properties. Because the expected collision velocity between cataloged objects in GEO shows a peak at a few hundred meters per second, those experiments were conducted at a velocity range less than 300 m/s. The model was formulated in a manner similar to what had been done in the area of hypervelocity impacts and was published by Yasaka and Hanada,[11] Hanada et al.,[12] and Yasaka et al.[13] Many international communities working on GEO space debris environment modeling have adopted their low-velocity collision model. They also have adopted the NASA standard breakup model 2000 revision because it is reported that the present GEO environment estimated with the NASA standard breakup model matches well with the observation result. They treat separately low- and hypervelocity collisions, however.

The purpose of this paper is to examine the applicability of the hypervelocity collision model included in the NASA standard breakup model to low-velocity collisions possible in GEO. Therefore, the experimental data from the mentioned low-velocity impact experiments will be reanalyzed and compared with the hypervelocity collision model. The analytic method is the same one used in the NASA standard breakup model 2000 revision. This paper will conclude that the NASA hypervelocity collision model can be applied to low-velocity collisions with some simple modifications.

NASA Standard Breakup Model

The NASA standard breakup model 2000 revision is quite different from other fragmentation models. Previously, mass and diameter (or size) were used interchangeably as the independent variable. However, with the incorporation of area-to-mass distributions, this interchangeability is lost, and then characteristic length L_C is chosen as the independent variable. The following subsections will describe the hypervelocity collision model adopted in the NASA standard breakup model 2000 revision according to Johnson et al.[14]

Size Distribution

Collisions between two satellites may be noncatastrophic, characterized primarily by fragmentation of the smaller object and by cratering of the larger object, or catastrophic, wherein both objects are totally fragmented. The difference between a catastrophic and a noncatastrophic collision is determined by the ratio of kinetic energy at impact to target mass. If the ratio is equal to or greater than 40 J/g, then the collision is catastrophic.

Based on several laboratory hypervelocity impact experiments, including the highly instrumented satellite orbital debris characterization impact test (SOCIT) series as well as the onorbit collision of the Solwind spacecraft, the number of fragments of a given size and larger can be described as

$$N(L_C) = 0.1(M)^{0.75}(L_C)^{-1.71} \tag{1}$$

In Eq. (1), the value of M is defined as the mass (in kilograms) of both objects in the case of a catastrophic collision. In the case of a noncatastrophic collision, the value of M is defined as the product of the mass (in kilograms) of the smaller object and the square of the collision velocity (in kilograms per second) with a proportional factor of 1 s^2/km^2, giving the ejecta mass (in kilograms). The smaller object is assumed to be destroyed in every collision, and its mass is added to the ejecta mass. Note that Eq. (1) and the following equations may be found their original form in Ref. 14.

Area-to-Mass Distribution

For objects with L_C smaller than 8 cm, a single area-to-mass ratio A/M distribution function has been derived from hypervelocity impact experiments as follows:

$$D^{\mathrm{SOC}}_{A/M}(\lambda_C, \chi) = N\left[\chi; \mu^{\mathrm{SOC}}(\lambda_C), \sigma^{\mathrm{SOC}}(\lambda_C)\right] \tag{2}$$

where

$$\lambda_C = \log_{10} L_C, \qquad \chi = \log_{10} A/M$$

and N is a normal distribution in χ about the mean value of

$$\mu^{\mathrm{SOC}}(\lambda_C) = \begin{cases} -0.3 & \lambda_C \le -1.75 \\ -0.3 - 1.4(\lambda_C + 1.75) & -1.75 \le \lambda_C < -1.25 \\ -1.0 & \lambda_C \ge -1.25 \end{cases}$$

with a standard deviation of

$$\sigma^{\mathrm{SOC}}(\lambda_C) = \begin{cases} 0.2 & \lambda_C \le -3.5 \\ 0.2 + 0.1333(\lambda_C + 3.5) & \lambda_C > -3.5 \end{cases}$$

Note that the A/M distribution function given by Eq. (2) is assumed to describe adequately the A/M characteristic of small debris produced in the explosive breakup of either spacecraft or rocket booster.

Average Cross-Sectional Area

The average cross-sectional area A_x is modeled as having a one-to-one correspondence with L_C: For characteristic length below 1.67 mm, a square is assumed to be the basic shape. For characteristic length above 1.67 mm, on the other hand, a square plate is assumed, with the thickness proportional to the side length of the square in millimeters to the power of 0.26. As a result, the size-to-area conversion yields

$$A_x = 0.540424 \cdot L_C^2, \qquad \text{where} \qquad L_C < 0.00167 \text{ m}$$

$$A_x = 0.556945 \cdot L_C^{2.0047077}, \qquad \text{where} \qquad L_C \ge 0.00167 \text{ m} \tag{3}$$

The conversion to mass M can be simply obtained by

$$M = A_x/(A/M)$$

Delta Velocity Distribution

When A/M is used as the independent variable instead of L_C, the ΔV (in meters per second) values were modeled as a normal distribution in $\nu = \log_{10} \Delta V$ about the mean value of

$$\mu^{\mathrm{COLL}}(\chi) = 0.9\chi + 2.9$$

with a standard deviation of

$$\sigma^{\mathrm{COLL}}(\chi) = 0.4$$

as follows:

$$D^{\mathrm{COLL}}_{\Delta V}(\chi, \nu) = N[\nu; \mu^{\mathrm{COLL}}(\chi), \sigma^{\mathrm{COLL}}(\chi)] \tag{4}$$

Low-Velocity Impact Experiments

Figure 1 shows an experimental facility at Kyushu University used by Harada[9] and Goto[10] to conduct low-velocity impact experiments. A single-stage air gun driven by a free piston was adopted to accelerate a projectile because of its simple and safe operation and associated low running cost. Its high-pressure reservoir of 300 mm in diameter with a length of 700 mm was designed to store the

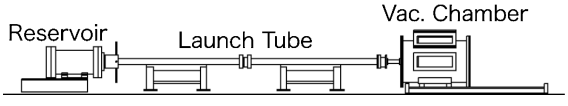

Fig. 1 Low-velocity impact experiment facility.

Table 1 Low-velocity impact experiments to analyze fragment size distribution

Shot	Velocity before hit, m/s	Ejecta mass, mg
21601	111.6	44.3
22401	111.6	50.0
20701	108.1	41.2
Average	110.4	45.2

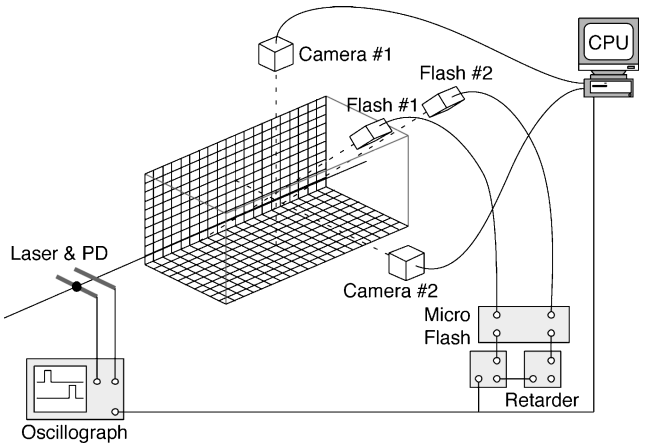

Fig. 2 Photographic system using high-resolution CCD cameras and two successive flashes.

pressurized air up to 7.5 MPa. Its launch tube has a length of 4000 mm and an inner diameter of 25 mm. Its vacuum chamber, with a degree of vacuum of 10^{-2} torr or lower, has a capacity of 600 mm in diameter with a length of 1000 mm, sufficient to observe the fragment creation process at and after impact.

Projectiles to be launched were stainless-steel spheres of 9 mm diameter. The air gun has a capability to launch these projectiles at velocities up to 300 m/s. Each projectile was centered in a sabot, which was removed at the sabot trap located in the forward direction of the launch tube. As shown in Fig. 2, two pairs of visible laser and photodiode module units located between the sabot trap and the observation chamber measured the projectile speed before impact.

The visualization technique adopted in these low-velocity impact experiments is simply photographing fragment creation process from two directions, horizontally and vertically, using two charge-coupled device (CCD) cameras and two successive flashes with time delays after the impact. Figure 2 includes a schematic of the photographing system. The camera head features a high-resolution CCD array containing 1008×1018 light-sensitive elements (effective pixels). The size of each pixel is 9×9 μm. Each exposure is started by a trigger signal generated by the digital oscillograph when the projectile intercepts the first laser light. After the CCD cameras take an exposure, the system makes two successive flashes of 2-μs duration to capture a sequence of the fragment creation process. The images captured by this system enable us to measure velocity decrement of the projectile after the impact and three-dimensional dispersion velocities of the fragments released from the target plate at the impact.

As typical of structures of GEO satellites, thin aluminum honeycomb sandwich shells with carbon fiber reinforced plastic (CFRP) face sheets, such as those used for body structures or rigid antenna reflectors, were prepared for the low-velocity impact experiments. Target samples were mounted on a rigid frame and then fixed in the vacuum chamber perpendicular to the trajectory of the projectile.

Tables 1 and 2 list impact scenarios conducted using the earlier mentioned experimental facility. Experiments listed in Table 1 were conducted to analyze fragment size distribution, whereas experiments listed in Table 2 were conducted to analyze fragment dispersion velocity distribution. In all laboratory experiments, the projectile penetrated the target plate and created a hole slightly larger in diameter than the projectile itself.

Table 2 Low-velocity impact experiments to analyze fragment delta velocity distribution

Shot	Velocity before hit, m/s	Velocity loss, m/s	Energy loss, J (%)
22113	145.0	8.3	3.5 (11.1)
22116	156.5	14.8	6.6 (18.0)
22120	143.9	11.9	4.9 (15.9)
22121	143.1	17.1	6.9 (22.5)
22122	148.6	18.6	7.8 (23.5)
22123	151.0	21.0	8.9 (25.9)
22124	148.8	16.8	7.1 (21.3)
Average	148.1	15.5	6.5 (19.8)

Table 3 Fragment characteristics from shot 20701

	Size	
Mass, mg	Long, mm	Short, mm
4.2	7.40	5.70
2.4	7.40	5.50
1.3	6.60	4.00
2.4	7.00	3.55
2.8	5.30	4.90
1.3	7.25	2.45
⋮	⋮	⋮

The total mass of the fragments created by each impact is shown in Table 1. Note that the projectile mass is not included in the ejecta mass because the projectile was retrieved without any damages. The number of fragments larger than 1 mm in size exceeds 100. More than 300 fragments smaller than 1 mm in size could be counted individually. Actual number of fragments can be estimated to be on the order of 1000. Note that a comparison of ejecta mass with the mass that the target lost after the impact indicates that only 2% of actual ejecta mass was not collected.

Projectile velocity decrement after each impact is shown in Table 2, as well as projectile energy loss. Projectile velocity after the impact was estimated from the images captured by the CCD cameras shown in Fig. 2. Table 2 shows that the projectiles lost only 10% of the initial velocity on average after the impact. This small decrement in projectile velocity through the impact means that the penetrating projectile causes other damages inside the impacted satellite.

Data Analysis and Discussion

Table 3 shows the experimental data from shot 20701, listed in Table 1. Fragment mass and two sizes (long and short) are listed in Table 3 but fragment thickness is not. According to Harada,[9] however, fragments from CFRP face sheets seem to keep their original thickness of 0.1 mm. Therefore, the thickness of fragments from CFRP face sheets can be assumed to be 0.1 mm. In addition, most fragments are plate-shaped with rectangular cross section. This information on fragment shape is useful to guess fragment thickness with known material density. In the following three subsections, size, average cross-sectional area, and area-to-mass distributions will be analyzed and discussed for shot 20701.

Size Distribution

Figure 3 shows a comparison of the fragment size distribution from shot 20701 with those given by Eq. (1), that is, the NASA size distribution model. To understand the effect of fragment thickness on the characteristic length, the size distribution for thickness-ignored fragments is shown as well. However, the difference is insignificant. Because this low-velocity impact can be considered as a noncatastrophic collision, the value of M in Eq. (1) is given by the product of the projectile mass and the square of the projectile velocity. Figure 3 indicates that Eq. (1) underestimates the cumulative number of fragments. This underestimation could be caused by the difference in mechanisms at impact. In these low-velocity impact experiments,

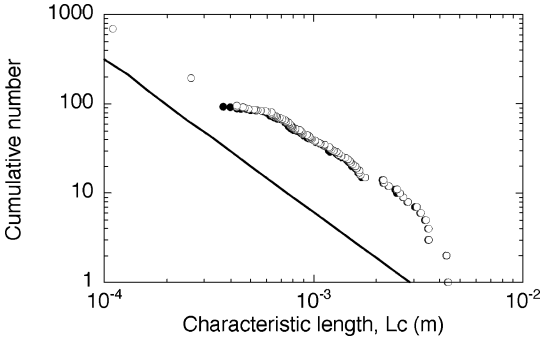

Fig. 3 Comparison of size distribution: ●, thickness ignored; ○, thickness guessed; and, ——, NASA size distribution model given by Eq. (1).

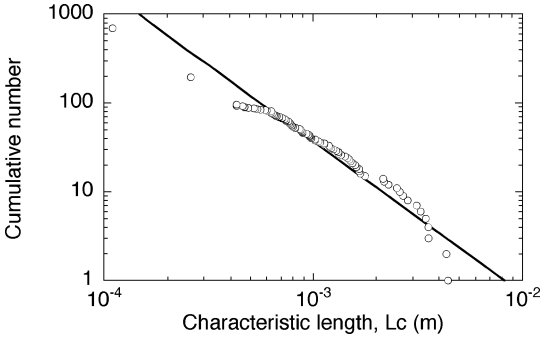

Fig. 4 Comparison of size distribution: ○, thickness guessed fragments and ——, Eq. (5) with $S = 6$.

the target plate was cracked into fragments without material phase change, whereas in hypervelocity impacts both the projectile and the target plate were melted and/or vaporized. However, the estimated ejecta mass matches well with the measured ejecta mass, and the slope given by Eq. (1) describes well the trend of the fragment size distribution. Therefore, a modification to be applied is only sifting Eq. (1) toward the greater size range. Figure 4 shows a modification based on

$$N(L_C) = S \cdot 0.1(M)^{0.75}(L_C)^{-1.71} \tag{5}$$

with $S = 6$.

Average Cross-Sectional Area

To estimate fragment average cross-sectional area, the following two equations are used in this analysis:

$$A_x = \tfrac{1}{3}(x \cdot y + y \cdot z + z \cdot x) \tag{6a}$$

$$A_x = \tfrac{1}{2}\left(L_C^2 + 2L_C \cdot z\right) \tag{6b}$$

Equation (6a) is based on a general technique developed for irregular-shaped fragments, whereas Eq. (6b) is developed for plate-shaped fragments and used in the NASA standard breakup model. As mentioned earlier, most fragments from this experiment are plate shaped so that Eq. (6b) would be best to estimate fragment average cross-sectional area. Figures 5a and 5b also indicate that the average cross-sectional area distribution estimated by Eq. (6b) matches well with the NASA size-to-area conversion model given by Eq. (3).

Area-to-Mass Distribution

Figure 6 shows a comparison of the area-to-mass distribution from shot 20701 with those given by Eq. (2), that is, the NASA area-to-mass distribution model. Note that the average cross-sectional area is estimated based on Eq. (6b). Most fragments show higher area-to-mass ratio than the NASA area-to-mass distribution. Fragments from CFRP face sheets show higher area-to-mass ratio and appear above $+3\sigma$, whereas other fragments from heavier materials show

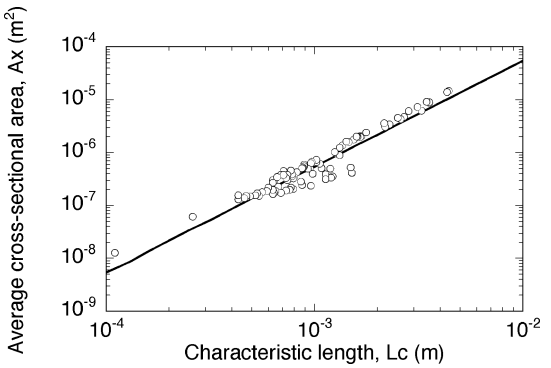

a) Estimate based on Eq. (6a)

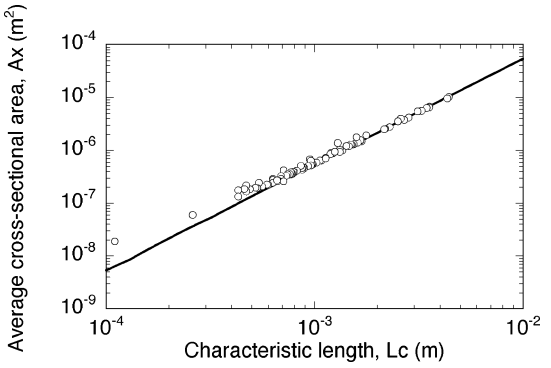

b) Estimate based on Eq. (6b)

Fig. 5 Comparison of average cross-sectional area: ——, NASA average cross-sectional area model given by Eq. (3).

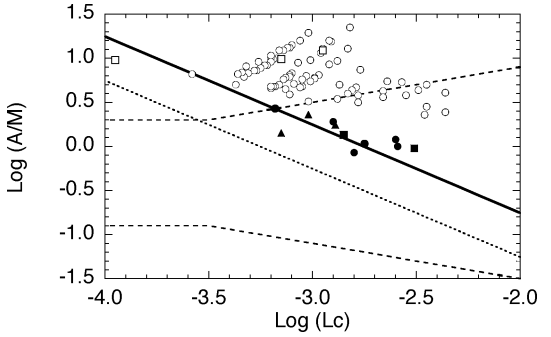

Fig. 6 Comparison of area-to-mass distribution: - - - -, NASA area-to-mass distribution within $\pm 3\sigma$; ——, Eq. (9) with density of CFRP; . . . . , Eq. (9) with density of aluminum alloy; ▲, Al fragment; ○, CFRP fragment; ●, CFRP+epoxy fragment; ■, CFRP+epoxy+Al; and □, fragment material not identified.

lower area-to-mass ratio and appear below $+3\sigma$. The difference in area-to-mass distribution could be caused by the difference in materials used in laboratory impact experiments. The aluminum honeycomb sandwich panels with CFRP face sheets used in these low-velocity impact experiments were not used in hypervelocity impact experiments.

Let assume that most fragments are plate shaped so that the average cross-sectional area of plate-shaped fragments can be estimated by Eq. (6b). The mass of plate-shaped fragments may be estimated by

$$M = \rho \cdot L_C^2 \cdot z \tag{7}$$

with known material density. From Eqs. (6b) and (7), we can evaluate the area-to-mass ratio by

$$A/M = (L_C/z + 2)/(2\rho \cdot L_C) \tag{8}$$

From the definition of the characteristic length, the ratio of the characteristic length to the fragment thickness should satisfy $L_C/z \geq 1$. Thus,

$$A/M \geq 1.5/(\rho \cdot L_C) \tag{9}$$

Equation (9) means that a lower boundary exists on the area-to-mass distribution as shown in Fig. 6. All fragments appear above the given lower boundaries. Therefore, the NASA area-to-mass distribution model can be applied with Eq. (9).

Delta Velocity Distribution

Table 4 shows the experimental data acquired from shot 22113 listed in Table 2. Table 4 shows fragment two-dimensional dispersion velocity but less information on fragment dimension and mass. It is quite difficult to estimate size distribution and area-to-mass distributions from Table 4. However, it can be assumed that area-to-mass distributions in these experiments are similar to those in shot 20701. This assumption of area-to-mass distribution enables us to show Fig. 7. The shaded area in Fig. 7 is a possible range of delta velocity with the assumed area-to-mass distribution. Although good correlation between the delta velocity distribution and the NASA delta velocity distribution model, that is, Eq. (4), cannot be observed, two modifications may be applied. One may be to modify Eq. (4) as demonstrated in Fig. 8, giving a normal distribution in χ about $\mu = 0.45\chi + 1.45$ with $\sigma = 0.27$. Another option is simply to apply Eq. (4) with the upper boundary of delta velocity derived from these experiments, that is, 1.3 times impact velocity. The latter is an easy way to apply the NASA delta velocity distribution model to low-velocity collisions.

Table 4 Fragment characteristics from shot 22113

Size, mm	Path angle, deg	Delta velocity, m/s
4.0	57.0	45.9
2.0	41.0	33.3
5.0	31.0	71.3
2.0	30.0	30.1
2.0	26.0	121.9
3.0	24.0	41.2
⋮	⋮	⋮

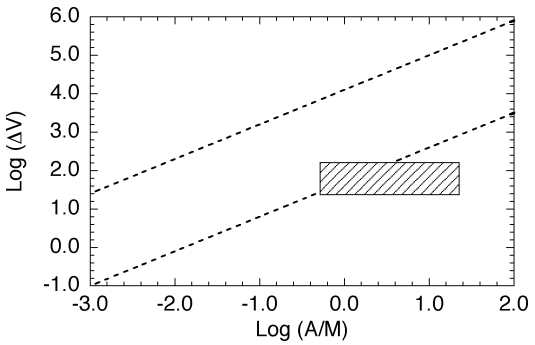

Fig. 7 Comparison of delta velocity distribution: - - - -, NASA delta velocity distribution within $\pm 3\sigma$ and shaded area, delta velocity distribution with assumed area-to-mass distribution.

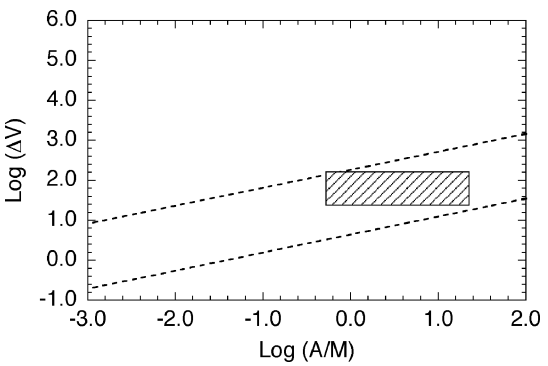

Fig. 8 Comparison of delta velocity distribution: - - - -, modified NASA delta velocity distribution within $\pm 3\sigma$ and shaded area, delta velocity distribution with assumed area-to-mass distribution.

Conclusions

This paper has reanalyzed the experimental data accumulated through low-velocity impact experiments performed at Kyushu University. The analytic method applied is the same as that used in the NASA standard breakup model 2000 revision. The comparison of the reanalyzed data with the hypervelocity collision model has indicated the following conclusions:

1) The NASA size distribution model describes adequately the trend of the fragments from the low-velocity impact experiments but should be modified to not underestimate the cumulative number of fragment.

2) The NASA size-to-area conversion model and the low-velocity impact experiments agree well.

3) The NASA area-to-mass distribution model can be applied with a theoretically derived lower boundary on area-to-mass distribution.

4) The NASA delta velocity distribution model can be applied with an experimentally derived upper boundary on delta-velocity distribution.

This paper has indicated that the hypervelocity collision model adopted in the NASA standard breakup model 2000 revision can be applied to low-velocity collisions with some modifications. However, additional low-velocity impact experiments will be required 1) to verify the applicability and modifications; 2) to examine the applicability and modifications at a slightly higher velocity range up to 1.5 km/s, that is, a maximum collision velocity between objects in the geosynchronous regime; and 3) to find where the transition from low- to hypervelocity collisions is. It is also required to examine the applicability of the modifications for noncatastrophic low-velocity collisions to catastrophic low-velocity collisions. The efforts will expand the versatility of the NASA standard breakup model to apply to all collisions possible in space.

Acknowledgments

The first author (T. Hanada) thanks Nicholas L. Johnson, Eric L. Christiansen, and members of the Orbital Debris Program Office of the NASA Johnson Space Center, Houston, Texas, for advice on the technical approach to analyze data from low-velocity impact experiments. This paper is based on IAC-03-IAA5.2.01 presented at the 54th International Astronautical Congress, Bremen, Germany, 29 September–3 October 2003.

References

[1]Bess, T. D., "Mass Distribution of Orbiting Man-Made Space Debris," NASA TN D-8108, Dec. 1975.

[2]Nebolsine, P. E., Lord, G. W., and Legne, H. H., "Debris Characterization Final Report," Physical Sciences, Inc., Rept. PSI TR-399, Andover, MA, Dec. 1983.

[3]Kling, R. L., "Postmortem of a Hypervelocity Impact: Summary," Teledyne Brown Engineering, Rept. CS86-LKD-001, Colorado Springs, CO, Sept. 1986.

[4]Kling, R. L., "The Collision of Satellites 16937 and 16938: Debris Characterization," Teledyne Brown Engineering, Rept. CS87-LKD-005, Colorado Springs, CO, May 1987.

[5]Johnson, N. L., "The Collision of Satellites 16937 and 16938: A Preliminary Report," Teledyne Brown Engineering, Rept. CS87-LKD-002, Colorado Springs, CO, Dec. 1986.

[6]McKnight, D. S., Johnson, N. L., Fudge, M. L., and Maclay, T. D., "Satellite Orbital Debris Characterization Impact Test (SOCIT) Series Data Collection Report," Kaman Sciences Corp., Contract NAS 9-19215, Alexandria, VA, April 1995.

[7]McKnight, D. S., Johnson, N. L., Fudge, M. L., and Maclay, T. D., "Analysis of SOCIT Debris Data and Correlation to NASA's Breakup Models," Kaman Sciences Corp., Contract NAS 9-19215, Alexandria, VA, July 1995.

[8]Friesen, L. J., Kessler, D. J., and Zook, H. A., "Reduced Debris Hazard Resulting From Stable Inclined Geosynchronous Orbit," *Advances in Space Research*, Vol. 13, No. 8, 1993, pp. 231–241.

[9]Harada, S., "Experiments of Simulating Space Debris Impacts at Geostationary Orbit," B. Eng. Dissertation, Dept. of Aeronautics and Astronautics, Kyushu Univ., Fukuoka, Japan, March 1996.

[10]Goto, K., "Dispersion Velocity Distribution Analysis of Fragments from Low-Velocity Impact," M. Eng. Dissertation, Dept. of Aeronautics and Astronautics, Kyushu Univ., Fukuoka, Japan, March 1997.

[11]Yasaka, T., and Hanada, T., "Low-Velocity Impact Test and Its Implications to Object Accumulation Model in GEO," *Advances in the Astronautical Sciences*, Vol. 91, 1996, pp. 1029–1038.

[12]Hanada, T., Yasaka, T., and Goto, K., "Fragments Creation via Impact at Low Speed," *Advances in the Astronautical Sciences*, Vol. 96, Univelt, San Diego, CA, 1997, pp. 979–986.

[13]Yasaka, T., Hanada, T., and Hirayama, H., "Low Velocity Projectile Impact on Spacecraft," *Acta Astronautica*, Vol. 47, No. 10, 2000, pp. 763–770.

[14]Johnson, N. L., Krisko, P. H., Liou, J.-C., and Anz-Meador, P. D., "NASA's New Breakup Model of EVOLVE 4.0," *Advances in Space Research*, Vol. 28, No. 9, 2001, pp. 1377–1384.

A. Ketsdever
Associate Editor